

## Tilting Styx and Nix but not Uranus with a Spin-Precession-Mean-motion resonance

Alice C. Quillen<sup>1</sup>, Yuan-Yuan Chen<sup>1,2</sup>,  
Benoît Noyelles<sup>3</sup>, & Santiago Loane<sup>1</sup>

the date of receipt and acceptance should be inserted later

**Abstract** A Hamiltonian model is constructed for the spin axis of a planet perturbed by a nearby planet with both planets in orbit about star. We expand the planet-planet gravitational potential perturbation to first order in orbital inclinations and eccentricities, finding terms describing spin resonances involving the spin precession rate and the two planetary mean motions. Convergent planetary migration allows the spinning planet to be captured into spin resonance. With initial obliquity near zero, the spin resonance can lift the planet's obliquity to near 90 or 180 degrees depending upon whether the spin resonance is first or zero-th order in inclination. Past capture of Uranus into such a spin resonance could give an alternative non-collisional scenario accounting for Uranus's high obliquity. However we find that the time spent in spin resonance must be so long that this scenario cannot be responsible for Uranus's high obliquity. Our model can be used to study spin resonance in satellite systems. Our Hamiltonian model explains how Styx and Nix can be tilted to high obliquity via outward migration of Charon, a phenomenon previously seen in numerical simulations.

**Keywords:** Planets and satellites: dynamical evolution and stability; celestial mechanics; Planets and satellites: individual: Styx; Planets and satellites: individual: Nix

---

<sup>1</sup>Department of Physics and Astronomy, University of Rochester, Rochester, NY 14627 USA  
E-mail: alice.quillen@rochester.edu

<sup>2</sup>Key Laboratory of Planetary Sciences, Purple Mountain Observatory, Chinese Academy of Sciences, Nanjing 210008, China

<sup>3</sup>Department of Mathematics and the Namur Centre for Complex Systems (naXys), University of Namur, 8 Rempart de la Vierge, Namur B-5000 Belgium

## 1 Introduction

Resonances involving planet or satellite spin can cause chaotic tumbling, prevent a body from tidally despinning or affect obliquity. Mercury was captured into a spin-orbit resonance, with spin rate a half integer multiple of its orbital mean motion, (e.g., [Goldreich & Peale(1966), Noyelles et al.(2014)]) whereas Hyperion is chaotically tumbling due to spin-orbit resonance overlap [Wisdom et al.(1984)]. Secular spin-orbit resonances occur when the period of precession of the spin axis of a planet is commensurate with (an integer multiple of) one of the periods of secular orbit variation [Ward(1974)]. Chaotic obliquity variations in Mars is attributed to secular spin resonances [Ward(1973), Ward(1974), Laskar & Robutel(1993), Touma & Wisdom(1993)]. Capture into the secular spin resonance connected to the vertical secular eigenfrequency associated with Neptune may have tilted Saturn’s obliquity to its current value of  $26.7^\circ$  [Ward & Hamilton(2004), Hamilton & Ward(2004)]. For an satellite in orbit about a binary such as Pluto and Charon, spin-binary resonance involves a commensurability between the binary mean motion, the orbital mean motion and the satellite spin rate [Correia et al.(2015)]. So far we have mentioned three-types of spin resonance: spin-orbit resonance (Mercury, Hyperion), spin secular resonance (Mars, Saturn) and spin-binary resonance.

Our numerical study of obliquity evolution of Pluto and Charon’s minor satellites, showed another type of spin resonance [Quillen et al.(2017)]. We found that a commensurability involving a mean motion resonance between Charon and a minor satellite and the satellite’s spin precession rate could influence its obliquity. For satellite Styx, near a 3:1 mean motion resonance with Charon, we saw obliquity variations when the angles

$$\begin{aligned}\phi_{s1} &= 3\lambda_{Styx} - \lambda_{Charon} - \dot{\phi}_{Styx} - \Omega_{Styx} \\ \phi_{s2} &= 3\lambda_{Styx} - \lambda_{Charon} - 2\dot{\phi}_{Styx}\end{aligned}\tag{1}$$

were librating about constant values rather than circulating. Here  $\lambda_{Styx}$  and  $\lambda_{Charon}$  are the mean longitudes of Styx and Charon and  $\Omega_{Styx}$  is the longitude of the ascending node of Styx. Orbital elements are measured with respect to Pluto or the center of mass of the Pluto/Charon binary, and its satellite orbital plane, not the Sun and the ecliptic. The precession angle  $\dot{\phi}_{Styx}$  describes the orientation of Styx’s spin axis with  $\dot{\phi}_{Styx} < 0$  as Styx’s spin axis precesses about the orbit normal.

The New Horizons Mission found that Pluto and Charon’s minor satellites, Styx, Nix, Kerberos and Hydra have not tidally spun down to near synchronous rotation and that all of them have high obliquities near  $90^\circ$  [Weaver et al.(2016)]. [Quillen et al.(2017)] suggested that the minor satellite current obliquities need not be primordial. A spin resonance involving a mean motion resonance between Charon and a minor satellite and the satellite’s spin precession rate, when drifting due to an outwards migrating Charon, can lift the obliquities of the minor satellites, accounting for their high and near  $90^\circ$  obliquities discovered by the New Horizons Mission.

As we were lacking a model for this type of spin resonance strength, we were unable to assess its strength or even identify which type of resonant angle was likely to be most important for each of Pluto and Charon's minor satellites. We address this issue here with the development of a Hamiltonian model for this spin resonance in section 2. In section 3 we explore resonance capture by allowing the resonance in our Hamiltonian model to drift. In section 4 we apply our model to Pluto and Charon's minor satellites.

Uranus has a high obliquity, of  $98^\circ$ . Could a similar spin resonance have tilted Uranus during a previous time when Uranus was in or near a mean motion resonance with another giant planet? Using the Hamiltonian model of sections 2 and 3 we answer this question in section 5. To aid the reader, a list of symbols is included in Table 1.

## 2 Spin evolution

A spinning oblate planet in orbit about a central mass  $M_*$  that has spin axis,  $\hat{\mathbf{s}}$ , tilted with respect to the orbit plane, precesses. We refer to the spinning object as a planet in orbit about a star, however we keep in mind that we can also consider a spinning satellite in orbit about a planet, asteroid or Kuiper belt object. We assume that the planet is rapidly spinning about its principal inertial axis and this is known as the *gyroscopic approximation*. The planet's moments of inertia are  $A, C$  with  $A > C$  and the planet's spin angular momentum is  $\mathbf{L}_s = wC\hat{\mathbf{s}}$  where  $w$  is the spin angular rotation rate and  $\hat{\mathbf{s}}$  is a unit vector. The planet's spin axis satisfies

$$\frac{d\hat{\mathbf{s}}}{dt} = \alpha_s(\hat{\mathbf{s}} \cdot \hat{\mathbf{n}})(\hat{\mathbf{s}} \times \hat{\mathbf{n}}) \quad (2)$$

[Colombo(1966)], with time derivatives taken with respect to the inertial frame. Here  $\hat{\mathbf{n}}$  is a unit vector perpendicular to the orbit plane, aligned with the orbital angular momentum vector. The precession rate

$$\alpha_s = \frac{3}{2} \frac{(C - A)}{Cw} \frac{n^2}{(1 - e^2)^{\frac{3}{2}}}, \quad (3)$$

where the orbital mean motion is  $n$  and the orbital eccentricity is  $e$ .

MacCullagh's formula gives the instantaneous torque on an oblate planet due to point mass  $M_*$

$$\mathbf{T} = 3(C - A) \frac{GM_*}{r^3} (\hat{\mathbf{r}} \cdot \hat{\mathbf{s}})(\hat{\mathbf{r}} \times \hat{\mathbf{s}}) \quad (4)$$

where  $\mathbf{r} = r\hat{\mathbf{r}}$  is the vector between the planet's center of mass and  $M_*$ . Equation 2 can be derived using MacCullagh's formula for the instantaneous torque by averaging over the orbit or computing  $\langle \mathbf{T} \rangle = \frac{1}{P} \int \mathbf{T} dt$  where the orbital period is  $P = 2\pi/n$ , and assuming that the planet remains spinning nearly about its principal axis [Colombo(1966)]. Thus equation 2 is consistent with

$$\frac{d\hat{\mathbf{s}}}{dt} = \frac{1}{Cw} \langle \mathbf{T} \rangle. \quad (5)$$

**Table 1** List of Symbols

$a$	semi-major axis
$e$	orbital eccentricity
$I$	orbital inclination
$\Omega$	longitude of the ascending node
$\omega$	argument of pericenter
$M$	mean anomaly
$\varpi = \omega + \Omega$	longitude of pericenter
$\lambda = M + \varpi$	mean longitude
$M_*$	mass of central star
$n$	mean motion
$\hat{\mathbf{n}}$	orbit normal unit vector
$\hat{\mathbf{s}}$	spin direction unit vector
$C, A$	moments of inertia of oblate planet
$w$	spin angular rotation rate of planet
$\alpha_s$	spin precession rate
$\alpha$	ratio of semi-major axes
$\mathbf{T}$	torque vector
$r$	orbital radius
$\phi$	spin precession angle
$\theta$	obliquity angle
$s \approx I/2$	used in low inclination expansions
$t$	time
$\tau$	normalized time
$R$	spinning planet's equatorial radius
$J_2$	second zonal gravity harmonic for the spinning planet
$q_s$	normalized quadrupole coefficient of satellite system
$l_s$	normalized angular momentum of satellite system
$\lambda_C$	normalized moment of inertia about principal axis
$p$	canonical momentum variable, a function of obliquity
$\Delta$	distance between perturber and spinning body
$\psi, \Psi$	angles used in expansion of disturbing function
$b_s^{(j)}(\alpha)$	Laplace coefficient
$j$	resonance index
$\epsilon$	resonance strength in a Hamiltonian model
$\nu$	distance to resonance in a Hamiltonian model
$c_0^j, c_s^j, c_{s'}^j$	coefficients used to compute spin resonance strengths
$c_{e1}^j, c_{e'1}^j$	"
$c_{e3}^j, c_{e'3}^j$	"
$\beta$	"

Due to secular perturbations arising from other planets, the orbit normal  $\hat{\mathbf{n}}$  is a function of time (e.g., [Colombo(1966), Ward(1975)]). A time dependent equation 2 has been used to study tidal evolution into Cassini states [Colombo(1966), Ward(1975)] and obliquity evolution of Mars [Ward(1973), Ward(1979), Bills(1990)] and Saturn [Ward & Hamilton(2004)]. Phenomena discovered and explored include capture into spin-secular resonance states (Saturn; [Ward & Hamilton(2004), Hamilton & Ward(2004)]) and chaotic obliquity evolution (Mars; [Ward(1973), Touma & Wisdom(1993), Laskar & Robutel(1993)]).

## 2.1 A Hamiltonian model for spin about a principal axis

Using angular spherical coordinates  $\phi, \theta$  in an inertial reference frame to specify the spin axis

$$\hat{\mathbf{s}} = (\cos \phi \sin \theta, \sin \phi \sin \theta, \cos \theta), \quad (6)$$

equation 2 can be written as a Hamiltonian dynamical system with canonical momentum  $p$ , conjugate to the precession angle  $\phi$

$$p = (1 - \cos \theta). \quad (7)$$

The Hamiltonian

$$H_{ave}(p, \phi) = \frac{\alpha_s}{2} (\hat{\mathbf{s}} \cdot \hat{\mathbf{n}})^2 \quad (8)$$

with  $\hat{\mathbf{s}}$  a function of  $p, \phi$ , (similar to that used by [Goldreich & Toomre(1969)] or [Ward & Rudy(1991)]). Hamilton's equations are

$$\dot{p} = -\frac{\partial H_{ave}}{\partial \phi} \quad (9)$$

$$\dot{\phi} = \frac{\partial H_{ave}}{\partial p} \quad (10)$$

and are equivalent to the equations of motion for the spin axis in equation 2.

With orbit normal  $\hat{\mathbf{n}}$  in the  $z$  direction, The angle  $\phi \in [0, 2\pi]$  describes spin precession.  $\theta \in [0, \pi]$  is the planet's obliquity. The canonical momentum  $p \in [0, 2]$  with  $p = 0$  at  $\theta = 0$ . With the addition of a third angle describing body orientation about the spin axis,  $\phi, \theta$  are Euler angles.

Equation 2 for  $d\hat{\mathbf{s}}/dt$  resembles equation 4 for  $\mathbf{T}$  but with  $\mathbf{r}$  replacing  $\hat{\mathbf{n}}$ . Because position vector  $\mathbf{r}$  is independent of the spin orientation angles  $\theta$  and  $\phi$ , the instantaneous spin vector (prior to averaging over the orbit) can also be described with a Hamiltonian system with

$$H(p, \phi) = -\frac{3}{2} \frac{(C - A) GM}{Cw} \frac{1}{r^3} (\hat{\mathbf{s}} \cdot \hat{\mathbf{r}})^2, \quad (11)$$

again with  $\hat{\mathbf{s}}$  a function of  $p, \phi$ . Hamilton's equations are equations of motion equivalent to

$$\frac{d\hat{\mathbf{s}}}{dt} = \frac{1}{Cw} \mathbf{T}. \quad (12)$$

When averaged over the orbit period this equation of motion for  $\hat{\mathbf{s}}$  is consistent with equation 2. The Hamiltonian in equation 11 can be averaged by writing  $r$  and  $\hat{\mathbf{r}}$  in terms of the mean anomaly and mean longitude and taking the average over these angles, yielding equation 8. The gyroscopic approximation should be a good one as long as the orbital period is much larger than the spin rotation period. For rigorous averaging calculations see [Boué & Laskar(2006)].

## 2.2 Precessional Constant with Satellites

An spinning oblate planet locks its satellites to its equator plane so that the system precesses as a unit [Goldreich(1965)]. The precession rate in equation 3 can be modified to take into account the satellites with

$$\alpha_s = \frac{3 n^2 J_2 + q_s}{2 w \lambda_C + l_s}, \quad (13)$$

[Ward(1975), French et al.(1993), Ward & Hamilton(2004)] but neglecting the orbital eccentricity. Here  $J_2$  is the coefficient of the second zonal gravity harmonic (from the quadrupole moment) of the planet's gravitational potential field and  $\lambda_C = C/mR^2$  is the planet's moment of inertia about its principal axis normalized to the product of planet mass and the square of the planet's equatorial radius. The parameter

$$l_s \equiv \sum_j \frac{m_j}{m} \left(\frac{a_j}{R}\right)^2 \frac{n_j}{w} \quad (14)$$

is the angular momentum of the satellite system normalized to  $mR^2w$  where  $m_j, a_j, n_j$  are the masses, semi-major axes (for the orbit about the planet) and mean motions of each satellite. The parameter

$$q_s \equiv \frac{1}{2} \sum_j \frac{m_j}{m} \left(\frac{a_j}{R}\right)^2 \frac{\sin(\theta - I_j)}{\sin \theta} \quad (15)$$

is the effective quadrupole coefficient of the satellite system with  $q_s/J_2$  being the ratio of the solar torque on the satellites to that directly exerted on the planet. Here  $\theta$  is the planet's obliquity and  $I_j$  the inclination of the  $j$ -th satellite with respect to the planet's equatorial plane. Without satellites  $q_s = l_s = 0$  and  $J_2 = (C - A)/(mR^2)$  so that equation 13 reduces to equation 3 at zero eccentricity.

## 2.3 A Perturbed Hamiltonian Model

We consider a spinning planet in orbit about a star at zero orbital inclination. Henceforth we take orbital normal  $\hat{\mathbf{n}} = \hat{\mathbf{z}}$ . When averaged over the orbit period and over the longitude of the ascending node the Hamiltonian describing the planet's spin (equation 8)

$$H_0(p, \phi) = \frac{\alpha_s}{2}(p - 1)^2 \quad (16)$$

and giving spin precession rate

$$\dot{\phi} = -\alpha_s \cos \theta \quad (17)$$

with  $\alpha_s$  as given in equation 13.

We consider a Hamiltonian model that includes a perturbation to  $H_0$ , in the form

$$H(p, \phi, t) = H_0(p) + H_1(p, \phi, t) \quad (18)$$

where  $H_1$  is a time dependent perturbation.

MacCullagh's formula gives the torque on our spinning planet due to a perturbing planet with mass  $m_p$ . The radial vector between the two planets is  $\mathbf{r} - \mathbf{r}_p$  where  $\mathbf{r}$  is the radial vector to the spinning planet (with respect to the central star) and  $\mathbf{r}_p$  the radial vector to the perturbing planet. The torque on the spinning planet is dependent upon the radial vector between the two planets

$$\mathbf{T} = 3(C - A) \frac{Gm_p}{|\mathbf{r} - \mathbf{r}_p|^5} ((\mathbf{r} - \mathbf{r}_p) \cdot \hat{\mathbf{s}}) ((\mathbf{r} - \mathbf{r}_p) \times \hat{\mathbf{s}}). \quad (19)$$

The perturbing planet is treated as a point mass. The associated Hamiltonian perturbation term (arising from  $\mathbf{T}$ ) is

$$H_1(p, \phi, t) = -\frac{3(C - A)}{Cw} \frac{Gm_p}{|\mathbf{r} - \mathbf{r}_p|^5} \frac{((\mathbf{r} - \mathbf{r}_p) \cdot \hat{\mathbf{s}})^2}{2} \quad (20)$$

and it is a time dependent perturbation as  $\mathbf{r}, \mathbf{r}_p$  vary.  $H_1 \ll H_0$  because the mass of the perturbing planet is much less than the mass of a star;  $m_p \ll M_*$ .

We describe the orbits in terms of orbital elements  $a, e, I, \Omega, M$  which are semi-major axis, eccentricity, inclination, longitude of the ascending node, argument of pericenter and mean anomaly, respectively. We also use the mean longitude  $\lambda = \Omega + \omega + M$  and the longitude of pericenter  $\varpi = \Omega + \omega$ . Our spinning and perturbing planets orbit a star with mass  $M_*$ .

Above  $\mathbf{r}$  and  $\mathbf{r}_p$  refer to positions of spinning and perturbing planets. We now depart from this notation, using  $\mathbf{r}$  and  $\mathbf{r}'$  to refer to radial vectors from the star of inner and outer orbiting masses. Orbital elements for the object with the *larger* semi-major axis will be referred to with a prime ( $a', e', I', \Omega', M', \lambda', \varpi'$ ) and those with the *smaller* semi-major axis without a prime. The ratio of semi-major axes  $\alpha \equiv a/a'$ . With radial vectors  $\mathbf{r}$  and  $\mathbf{r}'$  for inner and outer orbiting mass, equation 20 for the perturbation becomes

$$H_1(p, \phi, t) = -3 \frac{(C - A)}{Cw} n^2 \frac{m_p}{M_*} \frac{a_s^3}{|\mathbf{r} - \mathbf{r}'|^5} \frac{((\mathbf{r} - \mathbf{r}') \cdot \hat{\mathbf{s}})^2}{2} \quad (21)$$

where  $a_s$  is the semi-major axis of the spinning body,

$$a_s \equiv \begin{cases} a' & \text{for external spinning body} \\ a & \text{for internal spinning body.} \end{cases} \quad (22)$$

When the spinning body is external, we mean that it is perturbed by the mass  $m_p$  that has orbit interior to the spinning body.

Taking into account a satellite system around the spinning planet

$$\frac{(C - A)}{C} \rightarrow \frac{(J_2 + q_s)}{(\lambda_C + l_s)}$$

(comparing equation 3 with 13) and defining

$$\Delta \equiv |\mathbf{r} - \mathbf{r}'|, \quad (23)$$

we can write equation 21 as

$$H_1(p, \phi, t) = -\alpha_s \frac{m_p}{M_*} \left(\frac{a_s}{a'}\right)^3 \frac{a'^3}{\Delta^5} ((\mathbf{r} - \mathbf{r}') \cdot \hat{\mathbf{s}})^2 \quad (24)$$

with  $\alpha_s$  defined as in equation 13.

It is convenient to write time in terms of the precession constant with unitless  $\tau = \alpha_s t$ . The total Hamiltonian including perturbation (using equations 18, 16, 24)

$$H(p, \phi, \tau) = \frac{1}{2}(p-1)^2 - \beta \frac{a'^3}{\Delta^5} ((\mathbf{r} - \mathbf{r}') \cdot \hat{\mathbf{s}})^2 \quad (25)$$

with unitless coefficient

$$\beta \equiv \frac{m_p}{M_*} \left(\frac{a_s}{a'}\right)^3 \quad (26)$$

primarily dependent on the ratio  $m_p/M_*$  of perturbing planet and stellar masses.

#### 2.4 Evaluating the perturbation term in the Hamiltonian to first order in inclination

From the Hamiltonian in equation 25 we evaluate the rightmost term using the low eccentricity and inclination literal expansion method with Laplace coefficients described in section 6.4 by [Murray & Dermott(1999)]. We begin with radial vector  $\mathbf{r} = (x, y, z)$ , in terms of orbital elements

$$\mathbf{r} = r \begin{pmatrix} \cos \Omega \cos(\omega + f) - \sin \Omega \sin(\omega + f) \cos I \\ \sin \Omega \cos(\omega + f) + \cos \Omega \sin(\omega + f) \cos I \\ \sin(\omega + f) \sin I \end{pmatrix}, \quad (27)$$

and likewise for the other mass at  $\mathbf{r}'$  using primed orbital elements. As is customary at low inclination we let

$$\begin{aligned} \cos I &\approx 1 - I^2/2 \approx 1 - 2s^2 \\ \sin I &\approx I \approx 2s. \end{aligned}$$



To zero-th order in eccentricity and first order in inclination

$$\begin{aligned}
\frac{a'^3}{\Delta^5} ((\mathbf{r} - \mathbf{r}') \cdot \hat{\mathbf{s}})^2 \approx & \\
& \left\{ \frac{\sin^2 \theta}{2} \left[ 1 + \alpha^2 \right. \right. \\
& \quad + \alpha^2 \cos(2(\lambda - \phi)) + \cos(2(\lambda' - \phi)) \\
& \quad \left. \left. - 2\alpha \cos(\lambda + \lambda' - 2\phi) - 2\alpha \cos(\lambda - \lambda') \right] \right. \\
& + 2 \sin \theta \cos \theta \times \left[ \right. \\
& \quad s\alpha^2 \sin(2\lambda - \Omega - \phi) + s\alpha^2 \sin(\phi - \Omega) \\
& \quad + s' \sin(2\lambda' - \Omega' - \phi) + s' \sin(\phi - \Omega') \\
& \quad - s\alpha \sin(\lambda + \lambda' - \Omega - \phi) \\
& \quad - s\alpha \sin(\lambda - \lambda' - \Omega + \phi) \\
& \quad - s' \alpha \sin(\lambda + \lambda' - \Omega' - \phi) \\
& \quad \left. \left. + s' \alpha \sin(\lambda - \lambda' - \Omega' + \phi) \right] \right\} \\
& \times \frac{1}{2} \sum_{j=-\infty}^{\infty} b_{5/2}^{(j)}(\alpha) \cos(j(\lambda - \lambda')). \tag{28}
\end{aligned}$$

The non-secular terms with arguments that are not multiples of  $\lambda - \lambda'$  can be rewritten in terms of a single cosine or sine of orbital elements and  $\phi$ ;

$$\begin{aligned}
& \frac{\sin^2 \theta}{8} \left[ \cos(j\lambda - (j-2)\lambda' - 2\phi) \left( \alpha^2 b_{5/2}^{(j-2)} + b_{5/2}^{(j)} - 2\alpha b_{5/2}^{(j-1)} \right) \right. \\
& \quad \left. + \cos(j\lambda - (j+2)\lambda' + 2\phi) \left( \alpha^2 b_{5/2}^{(j+2)} + b_{5/2}^{(j)} - 2\alpha b_{5/2}^{(j+1)} \right) \right] \\
& + \frac{\sin \theta \cos \theta}{2} \times \left[ \right. \\
& \quad \sin(j\lambda - (j-2)\lambda' - \Omega' - \phi) (b_{5/2}^{(j)} - \alpha b_{5/2}^{(j-1)}) s' \\
& \quad - \sin(j\lambda - (j+2)\lambda' + \Omega' + \phi) (b_{5/2}^{(j)} - \alpha b_{5/2}^{(j+1)}) s' \\
& \quad + \sin(j\lambda - (j-2)\lambda' - \Omega - \phi) (\alpha^2 b_{5/2}^{(j-2)} - \alpha b_{5/2}^{(j-1)}) s \\
& \quad \left. - \sin(j\lambda - (j+2)\lambda' + \Omega + \phi) (\alpha^2 b_{5/2}^{(j+2)} - \alpha b_{5/2}^{(j+1)}) s \right]. \tag{29}
\end{aligned}$$

Arguments that are rapidly varying will not strongly perturb the spinning planet as they effectively average to zero. Only slowly varying arguments give resonantly strong perturbations. The external body has a slower mean motion than the internal one;  $n' < n$  recalling that  $n = \lambda$ . The slow arguments for positive  $j$  must be those containing  $j\lambda - (j+2)\lambda'$  and so are associated with second order mean motion resonances. Retaining only those three arguments

in equation 29 for a single positive  $j$  and using equations 28 and 29 we can write a near resonance Hamiltonian (equation 25) as

$$\begin{aligned}
H(p, \phi, \tau)^{j:j+2} &= \frac{1}{2}(p-1)^2 \\
&- \beta c_0^j p(2-p) \cos(j\lambda - (j+2)\lambda' + 2\phi) \\
&- (1-p)\sqrt{p(2-p)} \times \\
&\quad \left[ \beta c_s^j s \sin(j\lambda - (j+2)\lambda' + \Omega + \phi) \right. \\
&\quad \left. + \beta c_{s'}^j s' \sin(j\lambda - (j+2)\lambda' + \Omega' + \phi) \right], \tag{30}
\end{aligned}$$

where we have replaced  $\theta$  with  $p$  using

$$\begin{aligned}
\sin \theta \cos \theta &= (1-p)\sqrt{p(2-p)} \\
\sin^2 \theta &= p(2-p). \tag{31}
\end{aligned}$$

The unitless coefficients for  $j > 0$

$$\begin{aligned}
c_0^j(\alpha) &\equiv \frac{1}{4} \left( \alpha^2 b_{5/2}^{(j+2)}(\alpha) + b_{5/2}^{(j)}(\alpha) - 2\alpha b_{5/2}^{(j+1)}(\alpha) \right) \\
c_s^j(\alpha) &\equiv \left( \alpha b_{5/2}^{(j+1)}(\alpha) - \alpha^2 b_{5/2}^{(j+2)}(\alpha) \right) \\
c_{s'}^j(\alpha) &\equiv \left( \alpha b_{5/2}^{(j+1)}(\alpha) - b_{5/2}^{(j)}(\alpha) \right). \tag{32}
\end{aligned}$$

These coefficients are twice those in equation 29 because we have taken positive and negative  $j$  terms that give the same argument. We recall that time is in units of  $\alpha_s$ , as defined in equation 13, and the coefficient  $\beta$  depends on the mass ratio  $m_p/M_*$  (equation 26).

With a given  $j$ , to be near resonance  $jn \sim (j+2)n'$  or  $\alpha \sim \left(\frac{j}{j+2}\right)^{\frac{2}{3}}$ . To aid in applications we have computed the coefficients,  $c_0^j, c_s^j, c_{s'}^j$  for  $j = 1$  to 6 at near resonant semi-major axis ratios  $\alpha$  and their values are listed in Table 2.

Our Hamiltonian (equation 30) contains terms that are first order in orbital inclination. This is to be compared to first order mean motion orbital resonances that lack first order terms (in  $s$ ) in an expansion of the disturbing function and second order inclination mean motion resonances that by definition are proportional to  $s^2$ . Previous calculations of spin perturbations have considered the role of secular frequencies on planet spin orientation by considering how the orbit variations affect the torque from the star. In contrast here we have directly evaluated the torque from a nearby planet. The direct torque, computed here, is proportional to the mass of the perturbing planet (see equation 26). Secular perturbations scale with the masses of the planets in the system. So the sizes of these two types of spin-resonances are similar. We estimate that spin resonances associated with mean motion resonances are about as strong as secular spin resonances.

We could similarly consider how a nearby planet induces perturbations on the orbit of our spinning planet and then expand the equation for the torque from the star taking into account these perturbations. Variations in an expansion of the Hamiltonian in equation 11 due to perturbations on the orbit give terms with arguments similar to those computed here from an expansion of the Hamiltonian in equation 20. The orbit perturbations arising from the perturbing planet depends on the ratio  $m_p/M_*$  as does our  $\beta$ , but here our Hamiltonian perturbation contains both zeroth and first order terms in  $s$ . In contrast near a second order mean motion resonance orbital perturbations are second order in  $e$  and  $s$ . Because it contains zeroth and first order terms in the expansion, the torque directly exerted onto the spinning planet from a nearby planet should be stronger than variations on the torque from the star caused by orbital perturbations from a perturbing planet. We have neglected these orbital perturbations, but future work could take them into account.

In our numerical exploration of Styx we found two slowly moving angles,  $\phi_{s1}, \phi_{s2}$  (defined in equation 1) when there were obliquity variations. These angles can be recognized as arguments in the Hamiltonian in equation 30 with index  $j = 1$ , and identifying  $\lambda' = \lambda_{Styx}$  and  $\lambda = \lambda_{Charon}$ . Our perturbation computation gives terms with arguments consistent with the form we guessed from the slow moving angles we had seen in our simulations (see [Quillen et al.(2017)]). Our Hamiltonian model effectively describes the spin-resonance we saw in our numerical simulations.

## 2.5 Perturbation terms to first order in eccentricity

From the Hamiltonian in equation 25 we evaluate the rightmost term but keeping terms that are first order in orbital eccentricity and zeroth-order in inclination. Again we use the low eccentricity and inclination literal expansion method with Laplace coefficients described in section 6.4 by [Murray & Dermott(1999)].

**Table 2** Resonance coefficients

Resonance	$j$	$\alpha$	$c_0^j(\alpha)$	$c_s^j(\alpha)$	$c_{s'}^j(\alpha)$
3:1	1	0.481	0.765	1.782	-4.844
4:2	2	0.630	1.312	6.173	-11.423
5:3	3	0.711	2.027	14.270	-22.378
6:4	4	0.763	2.904	27.179	-38.793
7:5	5	0.799	3.941	45.999	-61.763
8:6	6	0.825	5.139	71.831	-92.386
Resonance	$j$	$\alpha$	$c_{e1}^j(\alpha)$	$c_{e'1}^j(\alpha)$	
2:1	1	0.630	-0.971	-0.384	
3:2	2	0.763	-2.862	-0.179	
4:3	3	0.825	-6.200	0.799	
5:4	4	0.862	-11.380	2.943	
6:5	5	0.886	-18.794	6.647	
7:6	6	0.902	-28.835	12.304	
Resonance	$j$	$\alpha$	$c_{e3}^j(\alpha)$	$c_{e'3}^j(\alpha)$	
4:1	1	0.397	-1.238	2.997	
5:2	2	0.543	-3.255	5.831	
6:3	3	0.630	-6.546	10.170	
7:4	4	0.689	-11.425	16.304	
8:5	5	0.731	-18.201	24.534	

These are coefficients defined in equations 32, 37, and 38. We used series expansions for the Laplace coefficients to compute them.

The first order in eccentricity terms that are added to equation 28;

$$\begin{aligned}
& \frac{a'^3((\mathbf{r} - \mathbf{r}') \cdot \hat{\mathbf{s}})^2}{\Delta^5} \approx \frac{\sin^2 \theta}{4} \left\{ \right. \\
& e\alpha^2 \left[ \cos(3\lambda - \varpi - 2\phi) \right. \\
& \quad \left. - 3 \cos(\lambda + \varpi - 2\phi) - 2 \cos(\lambda - \varpi) \right] \\
& - e\alpha \left[ \cos(2\lambda + \lambda' - \varpi - 2\phi) + \cos(2\lambda - \lambda' - \varpi) \right. \\
& \quad \left. - 3 \cos(\lambda' + \varpi - 2\phi) - 3 \cos(\lambda' - \varpi) \right] \\
& - e'\alpha \left[ \cos(2\lambda' + \lambda - \varpi' - 2\phi) + \cos(2\lambda' - \lambda - \varpi') \right. \\
& \quad \left. - 3 \cos(\lambda + \varpi' - 2\phi) - 3 \cos(\lambda - \varpi') \right] \\
& + e' \left[ \cos(3\lambda' - \varpi' - 2\phi) \right. \\
& \quad \left. - 3 \cos(\lambda' + \varpi' - 2\phi) - 2 \cos(\lambda' - \varpi') \right] \\
& \times \sum_{j=-\infty}^{\infty} b_{5/2}^{(j)}(\alpha) \cos(j\lambda - j\lambda')
\end{aligned}$$

$$\begin{aligned}
& + \left( 1 + \alpha^2 + \alpha^2 \cos(2\lambda - 2\phi) + \cos(2\lambda' - 2\phi) \right. \\
& \left. - 2\alpha \cos(\lambda + \lambda' - 2\phi) - 2\alpha \cos(\lambda - \lambda') \right) \\
& \times \sum_{j=-\infty}^{\infty} \left[ \right. \\
& \quad e \cos[(j+1)\lambda - j\lambda' - \varpi] \left( -\frac{\alpha}{2} D_\alpha + j \right) b_{5/2}^{(j)}(\alpha) \\
& \quad + e \cos[(j-1)\lambda - j\lambda' + \varpi] \left( -\frac{\alpha}{2} D_\alpha - j \right) b_{5/2}^{(j)}(\alpha) + \\
& \quad + e' \cos[j\lambda + (1-j)\lambda' - \varpi'] \left( \frac{\alpha}{2} D_\alpha + \frac{5}{2} - j \right) b_{5/2}^{(j)}(\alpha) \\
& \quad \left. + e' \cos[j\lambda - (1+j)\lambda' + \varpi'] \left( \frac{\alpha}{2} D_\alpha + \frac{5}{2} + j \right) b_{5/2}^{(j)}(\alpha) \right] \} \quad (33)
\end{aligned}$$

Combining arguments and taking only arguments that contain  $\phi$  these terms can be written

$$\begin{aligned}
& \cos[j\lambda - (j-3)\lambda' - \varpi - 2\phi] \frac{\sin^2 \theta}{8} e \left[ \alpha^2 \left( -\frac{\alpha}{2} D_\alpha + j - 2 \right) b_{5/2}^{(j-3)} + \alpha (\alpha D_\alpha - 2j + 3) b_{5/2}^{(j-2)} + \left( -\frac{\alpha}{2} D_\alpha + j - 1 \right) b_{5/2}^{(j-1)} \right] + \\
& \cos[j\lambda - (j+3)\lambda' + \varpi + 2\phi] \frac{\sin^2 \theta}{8} e \left[ \alpha^2 \left( -\frac{\alpha}{2} D_\alpha - j - 2 \right) b_{5/2}^{(j+3)} + \alpha (\alpha D_\alpha + 2j + 3) b_{5/2}^{(j+2)} + \left( -\frac{\alpha}{2} D_\alpha - j - 1 \right) b_{5/2}^{(j+1)} \right] + \\
& \cos[j\lambda - (j-3)\lambda' - \varpi' - 2\phi] \frac{\sin^2 \theta}{8} e' \left[ \alpha^2 \left( \frac{\alpha}{2} D_\alpha - j + \frac{9}{2} \right) b_{5/2}^{(j-2)} + \alpha (-\alpha D_\alpha + 2j - 8) b_{5/2}^{(j-1)} + \left( \frac{\alpha}{2} D_\alpha - j + \frac{7}{2} \right) b_{5/2}^{(j)} \right] + \\
& \cos[j\lambda - (j+3)\lambda' + \varpi' + 2\phi] \frac{\sin^2 \theta}{8} e' \left[ \alpha^2 \left( \frac{\alpha}{2} D_\alpha + j + \frac{9}{2} \right) b_{5/2}^{(j+2)} + \alpha (-\alpha D_\alpha - 2j - 8) b_{5/2}^{(j+1)} + \left( \frac{\alpha}{2} D_\alpha + j + \frac{7}{2} \right) b_{5/2}^{(j)} \right] + \\
& \cos[j\lambda - (j-1)\lambda' + \varpi - 2\phi] \frac{\sin^2 \theta}{8} e \left[ \alpha^2 \left( -\frac{\alpha}{2} D_\alpha - j - 2 \right) b_{5/2}^{(j-1)} + \alpha (\alpha D_\alpha + 2j + 3) b_{5/2}^{(j)} + \left( -\frac{\alpha}{2} D_\alpha - j - 1 \right) b_{5/2}^{(j+1)} \right] + \\
& \cos[j\lambda - (j+1)\lambda' - \varpi + 2\phi] \frac{\sin^2 \theta}{8} e \left[ \alpha^2 \left( -\frac{\alpha}{2} D_\alpha + j - 2 \right) b_{5/2}^{(j+1)} + \alpha (\alpha D_\alpha - 2j + 3) b_{5/2}^{(j)} + \left( -\frac{\alpha}{2} D_\alpha + j - 1 \right) b_{5/2}^{(j-1)} \right] + \\
& \cos[j\lambda - (j-1)\lambda' + \varpi' - 2\phi] \frac{\sin^2 \theta}{8} e' \left[ \alpha^2 \left( \frac{\alpha}{2} D_\alpha + j + \frac{1}{2} \right) b_{5/2}^{(j-2)} + \alpha (-\alpha D_\alpha - 2j) b_{5/2}^{(j-1)} + \left( \frac{\alpha}{2} D_\alpha + j - \frac{1}{2} \right) b_{5/2}^{(j)} \right] + \\
& \cos[j\lambda - (j+1)\lambda' - \varpi' + 2\phi] \frac{\sin^2 \theta}{8} e' \left[ \alpha^2 \left( \frac{\alpha}{2} D_\alpha - j + \frac{1}{2} \right) b_{5/2}^{(j+2)} + \alpha (-\alpha D_\alpha + 2j) b_{5/2}^{(j+1)} + \left( \frac{\alpha}{2} D_\alpha - j - \frac{1}{2} \right) b_{5/2}^{(j)} \right].
\end{aligned} \quad (34)$$

Inspection of the arguments in equation 34 implies that resonant terms will be important (with slowly varying arguments) near first order mean motion resonances, where  $j\lambda - (j+1)\lambda'$  is slowly varying (with positive  $j$ ) and near third order mean motion resonances, where  $j\lambda - (j+3)\lambda'$  is slowly varying. Near a third order mean motion resonance (and to first order in eccentricities

and inclinations) we can consider a near resonance Hamiltonian (similar to equation 30)

$$\begin{aligned}
H(p, \phi, \tau)^{j:j+3} &\approx \frac{1}{2}(p-1)^2 \\
&\quad - \beta c_{e3}^j e p (2-p) \cos[j\lambda - (j+3)\lambda' + \varpi + 2\phi] \\
&\quad - \beta c_{e'3}^j e' p (2-p) \cos[j\lambda - (j+3)\lambda' + \varpi' + 2\phi]. \tag{35}
\end{aligned}$$

Near a third order mean motion resonance, we can neglect the terms we previously computed (zero-th order in  $e, e'$  and first order in  $s, s'$ ) because they are only important near second order mean motion resonances. However, at higher order in  $e, e', s, s'$  additional terms will contribute near all of these mean motion resonances.

Near a third order mean motion resonance, equation 35 shows that the torque directly exerted by the planet is first order in eccentricity. The perturbing planet should cause orbital perturbations depending upon the third order of the eccentricity. So the variations in the torque from the star due to the orbit variations are likely to be smaller than the those caused directly from the torque of the perturbing planet.

Near a first order mean motion resonance

$$\begin{aligned}
H(p, \phi, \tau)^{j:j+1} &\approx \frac{1}{2}(p-1)^2 \\
&\quad - \beta c_0^{2j} p (2-p) \cos[2(j\lambda - (j+1)\lambda') + 2\phi] \\
&\quad - \beta c_s^{2j} s (1-p) \sqrt{p(2-p)} \sin[2(j\lambda - (j+1)\lambda') + \Omega + \phi] \\
&\quad - \beta c_{s'}^{2j} s' (1-p) \sqrt{p(2-p)} \sin[2(j\lambda - (j+1)\lambda') + \Omega' + \phi] \\
&\quad - \beta c_{e1}^j e p (2-p) \cos[j\lambda - (j+1)\lambda' - \varpi + 2\phi] \\
&\quad - \beta c_{e'1}^j e' p (2-p) \cos[j\lambda - (j+1)\lambda' - \varpi' + 2\phi]. \tag{36}
\end{aligned}$$

Here zero-th order and first order in inclination terms contribute but they are indexed by  $2j$  rather than  $j$ .

Near a first order mean motion resonance, equation 36 shows that the torque directly exerted by the planet is first order in eccentricity. The perturbing planet would also cause orbital perturbations that are first order in eccentricity. Variations in the torque from the star due to the orbit variations could be similar in size to those caused directly from the torque of the perturbing planet and these could be computed in future work.

The coefficients for Hamiltonians in equation 35 and 36 are twice those listed in equation 34 so as to include the contribution from a corresponding

negative  $j$  term that gives the same argument;

$$\begin{aligned}
c_{e3}^j &\equiv \frac{1}{4} \left[ \alpha^2 \left( -\frac{\alpha}{2} D_\alpha - j - 2 \right) b_{5/2}^{(j+3)} + \right. \\
&\quad \left. \alpha (\alpha D_\alpha + 2j + 3) b_{5/2}^{(j+2)} + \left( -\frac{\alpha}{2} D_\alpha - j - 1 \right) b_{5/2}^{(j+1)} \right] \\
c_{e'3}^j &\equiv \frac{1}{4} \left[ \alpha^2 \left( \frac{\alpha}{2} D_\alpha + j + \frac{9}{2} \right) b_{5/2}^{(j+2)} + \right. \\
&\quad \left. \alpha (-\alpha D_\alpha - 2j - 8) b_{5/2}^{(j+1)} + \left( \frac{\alpha}{2} D_\alpha + j + \frac{7}{2} \right) b_{5/2}^{(j)} \right] \quad (37)
\end{aligned}$$

and

$$\begin{aligned}
c_{e1}^j &\equiv \frac{1}{4} \left[ \alpha^2 \left( -\frac{\alpha}{2} D_\alpha + j - 2 \right) b_{5/2}^{(j+1)} + \right. \\
&\quad \left. \alpha (\alpha D_\alpha - 2j + 3) b_{5/2}^{(j)} + \left( -\frac{\alpha}{2} D_\alpha + j - 1 \right) b_{5/2}^{(j-1)} \right] \\
c_{e'1}^j &\equiv \frac{1}{4} \left[ \alpha^2 \left( \frac{\alpha}{2} D_\alpha - j + \frac{1}{2} \right) b_{5/2}^{(j+2)} + \right. \\
&\quad \left. \alpha (-\alpha D_\alpha + 2j) b_{5/2}^{(j+1)} + \left( \frac{\alpha}{2} D_\alpha - j - \frac{1}{2} \right) b_{5/2}^{(j)} \right]. \quad (38)
\end{aligned}$$

For low  $j$  we computed these coefficients and list them in Table 2.

Near a second order mean motion resonance ( $j : j + 2$ ) with  $j$  an odd integer, the first order in eccentricity terms do not contribute. Consequently equation 30 remains accurate to first order in eccentricity for odd  $j$  second order mean motion resonances.

### 3 Drifting Toy Hamiltonian models

The perturbations to the Hamiltonian arising from terms that are zero-th order in inclination and eccentricity are proportional to  $\sin^2 \theta$  (see equation 29). These would be important near first and second order mean motion resonances, as shown in the Hamiltonians in equations 30 and 36. Perturbations that are first order in eccentricity are also proportional to  $\sin^2 \theta$  (see equation 34) and these would be important near first and third order mean motion resonances (as in the Hamiltonians given in equation 35 and 36). In contrast perturbations that are first order in inclination are proportional to  $\sin \theta \cos \theta$  (see equation 29). These are relevant for first and second order mean motion resonances (as in the Hamiltonians given in equations 30 and 36). We have two types of perturbations, those proportional to  $\sin^2 \theta = p(2 - p)$  and those proportional to  $\sin \theta \cos \theta = (1 - p)\sqrt{p(2 - p)}$ . The level curves of these two types of Hamiltonians have different morphologies.

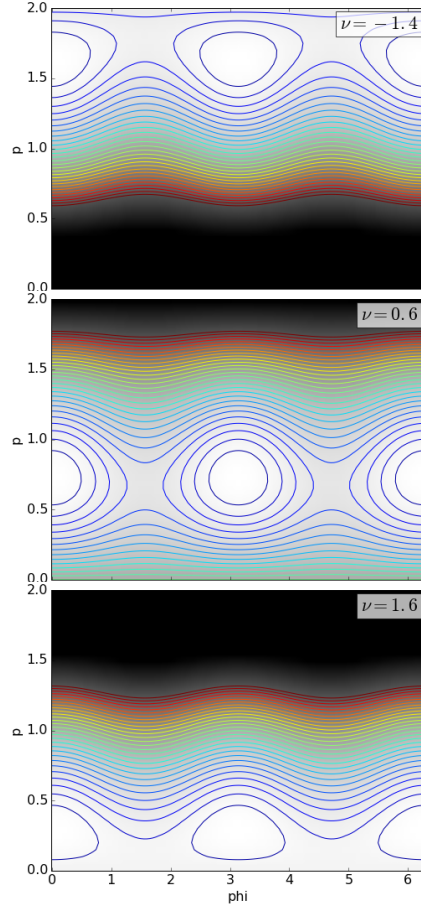


**Fig. 1** Level contours of the Hamiltonian in equation 43 with a perturbation proportional to  $\sin^2 \theta$  with resonance strength  $\epsilon = \beta c_0^j = 0.05$ . Each subplot shows level contours of the Hamiltonian with a different value of distance to resonance  $\nu_{2j}$  and with the value of  $\nu_{2j}$  labelled on the upper right. For  $|\nu_{2j}| < 2(1 + 2|\epsilon|)$  there are two stable fixed points at  $p$  value that increases with decreasing  $\nu_{2j}$ .

### 3.1 Hamiltonian model for a perturbation proportional to $\sin^2 \theta$

Taking the Hamiltonian in equation 30, appropriate for a second order mean motion resonance we define a frequency

$$\nu_{2j} \equiv \alpha_s^{-1}(jn - (j + 2)n'). \quad (39)$$

Here the spin precession frequency  $\alpha_s$  makes frequency  $\nu_{2j}$  unitless. Retaining a single  $j$  term zero-th order (in inclination) perturbation term, the Hamiltonian



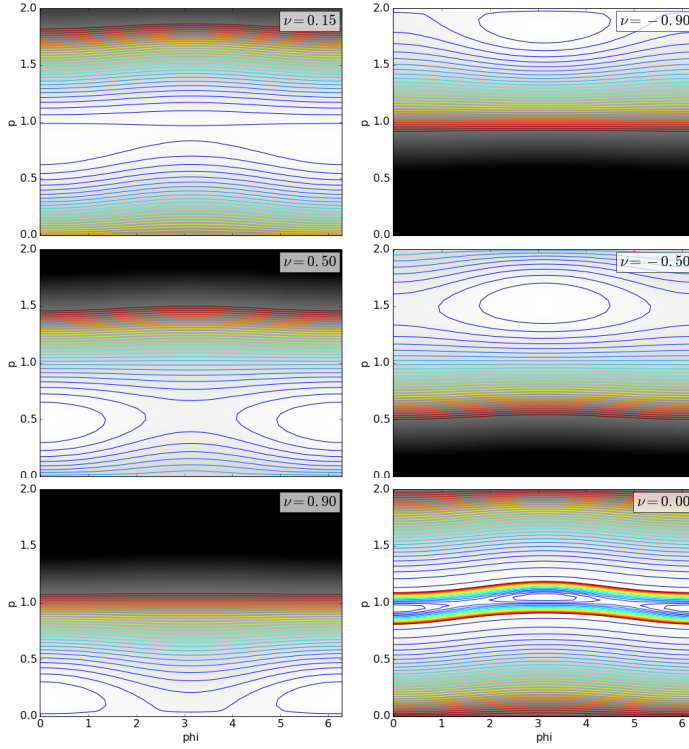


**Fig. 2** Level contours of the Hamiltonian in equation 50 with a term first order in inclination proportional to  $\sin \theta \cos \theta$ , with resonance strength  $\epsilon = \beta c_s^j s = 0.05$  and for different values of distance to resonance  $\nu_{2j_0}$ . This Figure is similar to Figure 1. For  $\nu_{2j_0} \gtrsim$  there is a stable fixed point at  $\varphi = 0$ . This one disappears just below  $\nu_{2j_0} = 0$ . For  $\nu_{2j_0} \lesssim 0$  there is a stable fixed point at  $\varphi = \pi$ . This one disappears just above  $\nu_{2j_0} = 0$ .

in equation 30 becomes

$$H(p, \phi, \tau)_{c0j} = \frac{1}{2}(p-1)^2 - \beta c_0^j p(2-p) \cos(\nu_{2j} \tau + 2\phi + c) \quad (40)$$

with  $c$  a constant phase.

A similar Hamiltonian would be derived near a first order mean motion resonance and retaining only a single first order in eccentricity term using the Hamiltonian in equation 36. In this case the relevant frequency (replacing  $\nu_{2j}$ ) would be one of the following  $\nu = \alpha_s^{-1}(2jn - 2(j+1)n' + \dot{\Omega})$ ,  $\alpha_s^{-1}(2jn - 2(j+1)n' + \dot{\Omega}')$ ,  $\alpha_s^{-1}(jn - (j+1)n' + \dot{\varpi})$  or  $\alpha_s^{-1}(jn - (j+1)n' + \dot{\varpi}')$  depending upon the argument. A Hamiltonian similar to equation 40 can also be derived near a third order mean motion resonance retaining only a single first order in eccentricity term and using the Hamiltonian in equation 35. In this case the relevant frequency would be  $\nu = \alpha_s^{-1}(jn - (j+3)n' + \varpi)$  or  $\alpha_s^{-1}(jn - (j+3)n' + \varpi')$ .

Performing a canonical transformation with time dependent generating function that is a function of old coordinates and a new momentum

$$F_2(\phi, p', \tau) = \frac{1}{2}(\nu_{2j}\tau + 2\phi + c)p', \quad (41)$$

giving new momentum  $p' = p$  equal to the old one and a new angle

$$\varphi = \frac{1}{2}(\nu_{2j}\tau + 2\phi + c). \quad (42)$$

Transforming the Hamiltonian in equation 40 we find a new Hamiltonian in these new coordinates

$$K(p, \varphi, \tau)_{c0j} = \frac{1}{2}(p-1)^2 + \frac{\nu_{2j}p}{2} - \epsilon p(2-p)\cos(2\varphi) \quad (43)$$

with

$$\epsilon \equiv \beta c_0^j. \quad (44)$$

The Hamiltonian is time independent as long as  $\nu_{2j}$  is fixed, and  $\nu_{2j}$  sets the distance to the center of resonance.

We can write the frequency (equation 39)

$$\nu_{2j} \frac{\alpha_s}{n} = j - (j+2) \left( \frac{a}{a'} \right)^{3/2}. \quad (45)$$

During an epoch of planet migration the semi-major axes  $a, a'$  may drift. When two planets approach each other either  $a$  increases or  $a'$  decreases so the frequency  $\nu_{2j}$  decreases. If the planet orbits separate,  $\nu_{2j}$  increases.

For various values of  $\nu_{2j}$  level curves for the Hamiltonian in equation 43 are shown in Figure 1. Fixed points are located at  $\varphi = 0, \pi$  and  $\varphi = \pm\pi/2$ . With  $\epsilon > 0$ , stable fixed points are at  $\varphi = 0, \pi$  whereas with  $\epsilon < 0$  they are at  $\varphi = \pm\pi/2$ . The stable ones are located at  $p = [1 + 2|\epsilon| - \nu/2]/(1 + 2|\epsilon|)$ , and there are no fixed points for  $|\nu_{2j}| > 2(1 + 2|\epsilon|)$ . The fixed point  $p$  value increases with decreasing frequency  $\nu_{2j}$ . At small  $\epsilon$ , the  $p$  value for the fixed points range from near 0 to near 2 corresponding to obliquity ranging from near 0 to near 180°.

We can mimic planet or satellite migration by allowing the frequency specifying distance to resonance  $\nu_{2j}$  to slowly vary. We let  $\nu_{2j}$  be linearly dependent on time. We note that  $\alpha_s$ , setting our unit of time and the strength of the coefficients, also depends on the semi-major axes and spin rate. For the moment we regard them as constants and allow only  $\nu_{2j}$  to vary. As  $\nu_{2j}$  decreases, corresponding to the planets migrating so that they approach one another, a planet initially at low obliquity could be captured into a stable fixed point and lifted in obliquity. Using Hamilton's equations for Hamiltonian of equation 43 and  $\epsilon = 0.01$ , we integrated a planet or satellite, within initial low  $p = 0.001$  (corresponding to an obliquity of  $\theta = 2.6^\circ$ ) and with  $\dot{\nu}_{2j} = -0.001$ . The time evolution of  $\theta, \varphi$  are shown in Figure 3. The planet is captured into a resonant region near a fixed point and lifted to an obliquity of near 180° and then it escapes resonance. The resonance strength we used is small. Even when the

resonance is weak and narrow, a planet or satellite could be captured into it and have its obliquity lifted to high values as the two planets approach each other and the resonance frequency drifts.

To lift a planet's obliquity from near 0 to 180°, the frequency  $\nu_{2j}$  must drop from approximately 2 to approximately  $-2$ . Using the definition for  $\nu_{2j}$  in equation 39, the frequency  $\nu_{2j}\alpha_s = jn - (j+2)n'$  should drop from  $2\alpha_s$  to  $-2\alpha_s$  to lift an initially low obliquity planet to high obliquity. If the precession frequency is slow because the planet is nearly spherical, or is spinning rapidly and has a compact satellite system, then the required extent of planetary migration would be small.

In this section we have assumed that resonance strength is time independent, however if the spinning planet migrates or spins down,  $\alpha_s$  is a function of time and we have neglected this variation here. The ratio of semi-major axes  $\alpha$  is also a function of time during migration. These variations could be taken into account in applications of our toy model by allowing the resonance strength to be time dependent.

### 3.2 Hamiltonian model for a perturbation proportional to $\sin\theta\cos\theta$

We now consider a Hamiltonian model with a single perturbation proportional to  $\sin\theta\cos\theta$ . We retain a single  $j$  term first order in inclination in the Hamiltonian 30. Using a frequency

$$\nu_{2jo} \equiv \alpha_s^{-1}(jn - (j+2)n' + \Omega) \quad (46)$$

we have a simplified Hamiltonian

$$\begin{aligned} H(p, \phi, \tau)_{csj} &= \frac{1}{2}(p-1)^2 \\ &\quad - \beta c_s^j s(1-p)\sqrt{p(2-p)}\sin(\nu_{2jo}\tau + \phi + c) \end{aligned} \quad (47)$$

with constant  $c$ . Using a canonical coordinate transformation with generating function

$$F_2(\phi, p', \tau) = (\nu_{2jo}\tau + \phi + c)p', \quad (48)$$

we derive a new angle

$$\varphi = \nu_{2jo}\tau + \phi + c \quad (49)$$

and a new Hamiltonian

$$K(p, \varphi, \tau)_{csj} = \frac{1}{2}(p-1)^2 + \nu_{2jo}p - \epsilon(1-p)\sqrt{p(2-p)}\cos\varphi \quad (50)$$

with resonance strength

$$\epsilon \equiv \beta c_s^j s. \quad (51)$$

The Hamiltonian would look the same if a first order term proportional to  $s'$  were used with frequency  $\nu = \alpha_s^{-1}(jn - (j+2)n' + \Omega')$  instead of  $\alpha_s^{-1}(jn - (j+2)n' + \Omega)$ , and with perturbation strength,  $\epsilon$ , equal to  $\beta c_s^j s'$  instead of

$\beta c_s^j$ s. A similar Hamiltonian would be derived near a first order mean motion resonance and using a single  $j$  term that is first order in inclination from the Hamiltonian in equation 36.

Level curves for the Hamiltonian in equation 50 are shown in Figure 2 for different values of  $\nu_{2j_0}$  and for  $\epsilon = 0.05$ . Fixed points satisfy

$$\nu_{2j_0} = -q \pm \epsilon \frac{(1 - 2q^2)}{\sqrt{1 - q^2}} \quad (52)$$

with  $q \equiv 1 - p$  and the sign of  $\epsilon$  is positive for the fixed points at  $\phi = 0$  and negative for those at  $\phi = \pi$ . For  $\nu_{2j_0} \lesssim 0$  a stable fixed point is at  $\varphi = 0$  and has  $p < 1$ . However just above  $\nu_{2j_0} = 0$  this fixed point disappears. For  $\nu_{2j_0} \gtrsim 0$  there is again a stable fixed point but at  $p > 1$ . This one disappears just below  $\nu_{2j_0} = 0$ . Near  $\nu_{2j_0} = 0$ , two stable fixed points are present at  $\phi = 0, \pi$  and the resonant islands are small.

As before we integrate the equations of motion for a slowly drifting system. We plot a planet trajectory in Figure 4 using the Hamiltonian in equation 50,  $\epsilon = 0.01$ ,  $\dot{\nu}_{2j_0} = -0.001$ , initial conditions  $(\varphi, p) = (1.5, 0.001)$  and  $\nu_{2j_0} = 1.4$ . Again we find that resonance capture is possible for a particle initially at low obliquity. However because the fixed point disappears near an obliquity of  $90^\circ$  the planet must escape resonance near this value rather than near  $180^\circ$  as for the perturbation that is proportional to  $\sin^2 \theta$  (explored in subsection 3.1).

In this section we have assumed that resonance strength is time independent. However variation in semi-major axis ratio,  $\alpha$ , precession rate  $\alpha_s$  and orbital inclination can affect the resonance strength.

### 3.3 Adiabatic Limits for Resonance Capture

When the drift from migration is too fast or not adiabatic, a particle in orbit will jump across mean motion resonance rather than capture into resonance [Quillen(2006)]. At drift rates below a critical drift rate, the resonance can capture at high probability. This critical drift rate is approximately equal to the square of the resonance libration frequency [Quillen(2006)]. There is a critical initial eccentricity, below which capture into mean motion resonance is assured when drift is adiabatic [Borderies & Goldreich(1984)]. The drift rate defining the adiabatic limit and the limiting eccentricity ensuring capture can be estimated from the Hamiltonian by considering the dimensions of the coefficients [Quillen(2006)]. By considering the form of the Hamiltonians in equations 43, 50 at low  $p$  we can similarly estimate the drift rate required for capture into spin resonance.

At low  $p$  (low obliquity) the perturbation term in the Hamiltonian of equation 43 (with perturbation  $\propto \sin^2 \theta$ ) is proportional to  $\epsilon 2p \cos 2\phi$ , so the drifting resonance behaves like a second order mean motion resonance that is proportional to  $e^2$  or the Poincaré momentum variable  $\Gamma$ . The resonance libration frequency at low  $p$  is  $\omega_{lib} \propto |\epsilon|$ . In analogy to the Hamiltonian for mean motion resonance, we expect that capture into resonance for the drifting Hamiltonian

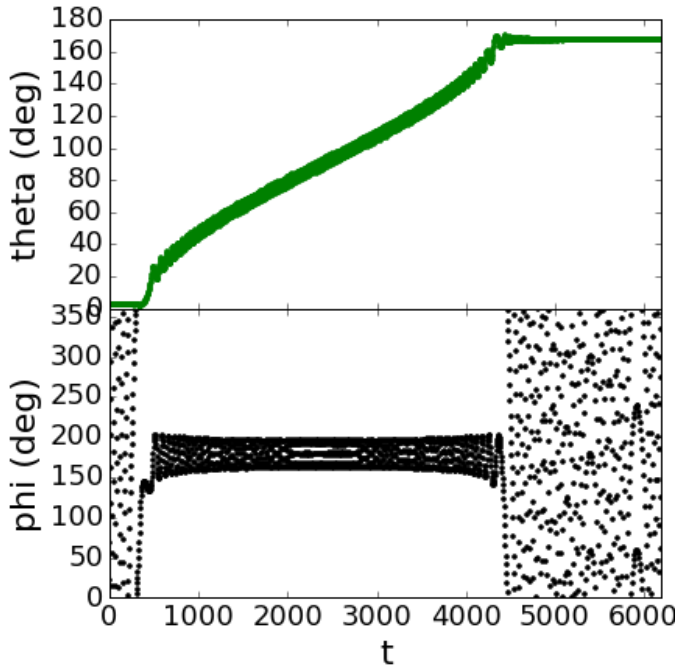


**Fig. 3** Integration of the Hamiltonian in equation 43 with a zero-th order perturbation (in inclination)  $\propto \sin^2 \theta$  and resonance strength  $\epsilon = 0.01$ . Here the resonance drifts with  $\dot{\nu}_{2j} = -0.001$  corresponding to the planets slowly migrating closer together. Initial conditions are  $(\varphi, p) = (0.4, 0.001)$ , and  $\nu_{2j} = 2.4$ . The top panel shows obliquity as a function of time whereas the bottom panel shows the precession angle. The integrated body is captured into spin resonance at low obliquity and exits near an obliquity of  $180^\circ$ .

of equation 43 is likely for drift rates  $|\dot{\nu}_{2j}| \lesssim \epsilon^2$  (the square of the libration frequency, and following [Quillen(2006), Mustill & Wyatt(2011)]) and for initial momentum  $p \lesssim |\epsilon|$  (the critical momentum below which capture is assured for adiabatic drift; see [Borderies & Goldreich(1984), Quillen(2006)]).

In contrast the resonant term for the Hamiltonian in 50, with perturbation  $\propto \sin \theta \cos \theta$ , at low  $p$  is proportional to  $\sqrt{p}$  and so this resembles a first order mean motion resonance, proportional to  $e$  or the square root of the Poincaré momentum variable,  $\sqrt{T}$ . The libration frequency  $\omega_{lib} \propto |\epsilon|^{\frac{2}{3}}$  (following [Quillen(2006), Mustill & Wyatt(2011)]). The resonance should capture at a drift rate  $|\dot{\nu}_{2j0}| \lesssim |\epsilon|^{\frac{4}{3}}$  (the square of the libration frequency) and for initial  $p \lesssim |\epsilon|^{\frac{2}{3}}$ .

To estimate coefficients for the limits we show capture probabilities for a range of drift rates (different  $\dot{\nu}_{2j}, \dot{\nu}_{2j0}$  values) for the Hamiltonians in equations 43 and 50 in Figure 5. In both cases we set perturbation strength  $\epsilon = 0.01$ . We computed the capture probabilities for three different initial  $p$  values, 0.001, 0.01, and 0.1 corresponding to initial obliquities of  $2.6^\circ$ ,  $8.1^\circ$  and  $26^\circ$ . Each point shown in Figure 5 was computed from an average of 30 integrations

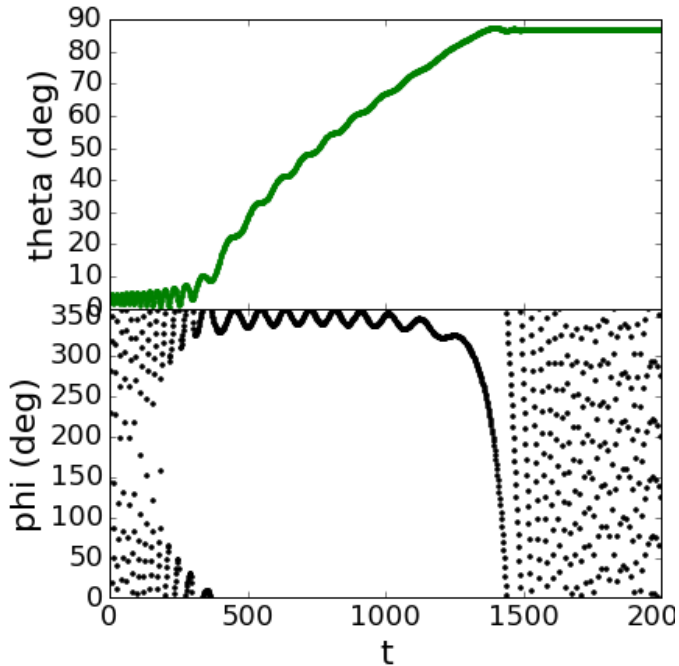


**Fig. 4** Integration of the Hamiltonian in equation 50 with a first order perturbation (in inclination) proportional to  $\sin \theta \cos \theta$  and resonance strength  $\epsilon = 0.01$ . Here the resonance drifts with  $\dot{\nu}_{2j_0} = -0.001$  for planets slowly migrating closer together. Initial conditions are  $(\phi, p) = (1.5, 0.001)$ , and  $\nu_{2j_0} = 1.4$ . The top panel shows obliquity as a function of time whereas the bottom panel shows the precession angle. The integrated body is captured into spin resonance at low obliquity and exits near an obliquity of  $90^\circ$ .

where each integration was begun outside of resonance at a randomly chosen initial  $\phi$ , chosen from a uniform distribution spanning  $[0, 2\pi]$ . The scatter likely arises from dependence on phase when the drifting system reaches resonance [Quillen(2006), Mustill & Wyatt(2011)]. To reduce dependence on phase and reduce scatter in these plots we also chose random initial  $\nu_{2j}, \nu_{2j_0}$  values, ensuring that we began outside of resonance and from a uniform distribution with a width of 0.5. For those integrations that captured into spin resonance (as determined by a large increase in obliquity or  $p$ ) we computed the mean final obliquity (of the integrations that captured into resonance) and these are shown as points on the bottom panels in Figure 5. The solid lines show fits of a hyperbolic tangent function to the capture probability and are used to determine where the transition from low to high probability takes place.

Figure 5 shows that for low initial  $p$  capture takes place at  $|\dot{\nu}_{2j}| \sim 10^{-3}$  for the  $\sin^2 \theta$  resonance with Hamiltonian in equation 43. Using the dependence on  $\epsilon^2$  we estimate that

$$|\dot{\nu}_{2j}|_{\sin^2 \theta} \lesssim 10\epsilon^2 \quad (53)$$

for capture into the  $\sin^2 \theta$  resonance.

Capture takes place at  $|\dot{\nu}_{2jo}| \sim 4 \times 10^{-3}$  for the  $\sin \theta \cos \theta$  resonance (Hamiltonian of equation 50) giving

$$|\dot{\nu}_{2jo}|_{\sin \theta \cos \theta} \lesssim 2|\epsilon|^{4/3} \quad (54)$$

for capture into the  $\sin \theta \cos \theta$  resonance.

The  $\sin \theta \cos \theta$  resonance (Figure 5b) exhibits a sharper sensitivity to drift rate than the  $\sin^2 \theta$  one (Figure 5a), consistent with previous studies showing that first order mean motion resonances have a more abrupt transition in capture probability near the adiabatic limit [Quillen(2006)].

Following resonance capture, Figure 5 shows that after escaping resonance the final obliquity is somewhat sensitive to initial obliquity and drift rate. For the  $\sin^2 \theta$  resonance, higher initial obliquity gave lower final obliquity after resonance capture. For both types of resonances, nearer the adiabatic limit and at higher drift rates, the final obliquities are somewhat lower.

How long does it take to lift the obliquity in one of these spin resonances? For the  $\sin^2 \theta$  resonance, once captured into resonance,  $p$  must drift from 0 to 2. Within a factor of a few the total time in resonance is  $1/|\dot{\nu}_{2j}|$ . For the  $\sin \theta \cos \theta$  resonance the total time in resonance is equivalent. Restoring units, once captured into resonance at low obliquity, the time to lift the obliquity to near  $180^\circ$  for the  $\sin^2 \theta$  resonance or near  $90^\circ$  for the  $\sin \theta \cos \theta$  resonance is

$$t_{lift} \sim \frac{1}{|\dot{\nu}| \alpha_s}. \quad (55)$$

where  $\nu$  is the appropriate frequency (either  $\nu_{2j}$  or  $\nu_{2jo}$ ).

We consider how the distance to spin resonance,  $\nu$ , might vary when two planets are in mean motion resonance and migrating. Once captured into mean motion resonance, eccentricity or and inclination can continue to increase as the system migrates. While in resonance, a resonant argument librates about a constant value. For example, an inclination 3:1 mean motion resonance contains the argument  $\lambda - 3\lambda' + 2\Omega$ . With this argument librating the frequency  $\omega = n - 3n' + 2\dot{\Omega}$  approximately averages to zero. However, the frequencies setting distance to the spin resonance near the second-order mean motion resonance,  $\nu_{2j}$  or  $\nu_{2jo}$ , are not the same as  $\omega$ . The difference between  $\nu_{2j}$  and  $\omega$  is  $2\dot{\Omega}$  for the spin resonance  $\propto \sin^2 \theta$  and the difference between  $\nu_{2jo}$  and  $\omega$  is  $\dot{\Omega}$  for the spin resonance  $\propto \sin \theta \cos \theta$ . The precession rate  $\dot{\Omega}$  is sensitive to inclination and would vary if the orbital inclination increases within mean motion resonance. The same is true for  $\dot{\varpi}$  as eccentricity increases within mean motion resonance. As the orbital inclination or eccentricity increases within mean motion resonance, the frequencies setting the distance to spin resonances would vary. As spin resonance frequencies can vary for a body evolving within a mean motion resonance, spin resonances can be encountered, causing either spin resonance capture or a jump in obliquity as the spin resonance is crossed.

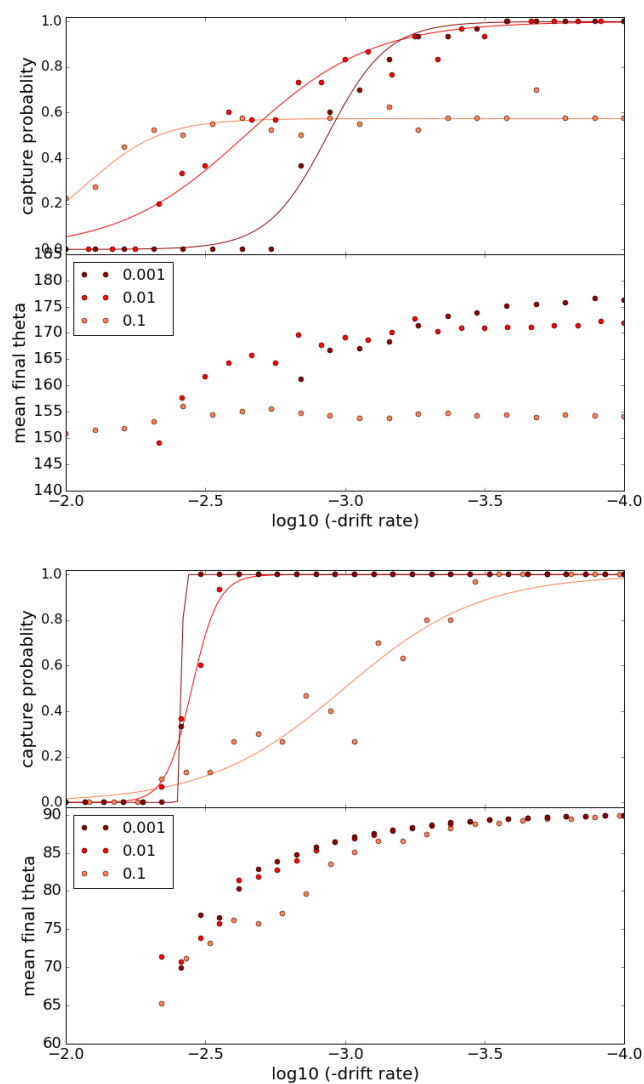


**Fig. 5** a) The top panel shows capture probabilities for the Hamiltonian in equation 43 with resonant term  $\propto \sin^2 \theta$  with resonance strength  $\epsilon = 0.01$  as a function of drift rate for three different initial obliquities or  $p$  values. The initial  $p$  values 0.001, 0.01, 0.1, shown in the key on the lower left, correspond to initial obliquities of 2.6, 8.1 and 26°. The bottom panel shows the average final obliquities (in degrees) when capture took place for the same initial  $p$  values. The  $x$  axes show the  $\log_{10}$  of the absolute value of the drift rate  $|\dot{\nu}_{2j}|$ . The drift rate is higher on the left hand side and gives lower capture probabilities. Each point is computed from an average of 30 integrations. b) Similar to a) except for the Hamiltonian in equation 50, with resonant term  $\propto \sin \theta \cos \theta$  and with  $x$  axis showing  $\log_{10} |\dot{\nu}_{2jo}|$ .



#### 4 Application to Pluto and Charon's minor satellites

We consider spinning minor satellites Styx and Nix, that have orbits exterior to Charon. With an exterior spinning body, the unitless coefficient  $\beta$  (defined in equation 26) is approximately equal to the mass ratio of Charon and Pluto,  $\beta \sim 0.1$ . Styx is near the 3:1 mean motion resonance with Charon and Nix near the 4:1 mean motion resonance with Charon.

We first consider Styx, with an orbital period of 20 days. As Styx is near the 3:1 second order mean motion resonance we consider the Hamiltonian in equation 30 with  $j = 1$ . Inspection of Table 2 shows that there is a zero-th order (in inclination and eccentricity) perturbation with coefficient  $c_0^1(\alpha) = 0.76$  giving a resonance term  $\propto \sin^2 \theta$ . There are two terms first order in orbital inclination with larger coefficients,  $c_s^1 = 1.782$  and  $c_{s'}^1 = -4.84$  and giving resonance terms  $\propto \sin \theta \cos \theta$ . The  $c_0$  term need only be multiplied by  $\beta$  giving resonance strength  $\epsilon = 0.1 \times 0.76 = 0.08$  for the Hamiltonian in equation 43. The  $c_s^1$  and  $c_{s'}^1$  coefficients should be multiplied by the orbital inclinations of Styx and Charon, respectively, to estimate the strength of the  $\sin \theta \cos \theta$  resonance. Working in a coordinate frame aligned with Styx's orbit (and with the obliquity measured with respect to Styx's orbit normal), we use the inclination of Charon and need only the  $c_{s'}^1$  coefficient. Taking into account  $\beta = 0.1$ , we estimate a resonance coefficient strength  $\epsilon = 0.1 \times c_{s'}^1 = 0.48 I_{Charon}$  where  $I_{Charon}$  is the inclination of Charon's orbit relative to Styx's. With an inclination of  $I_{Charon} = 6^\circ = 0.1$  radians we find  $\epsilon = 0.05$ . The resonant perturbation term is  $\propto \sin \theta \cos \theta$  and the relevant Hamiltonian is equation 50.

The two resonance strengths,  $\propto \sin^2 \theta$  and that  $\propto \sin \theta \cos \theta$ , have similar strengths when Charon's inclination is  $\sim 8^\circ$ . With a moderate inclination, the  $c_{s'}^1$  resonance might be more important than the  $c_0^1$  one. After capture, Styx should exit the  $\sin \theta \cos \theta$  resonance with an obliquity near  $90^\circ$ , as we saw in our simulations (section 5 by [Quillen et al.(2017)]) and as illustrated in Figure 4. In contrast after capture into the  $c_0$  resonance,  $\propto \sin^2 \theta$ , Styx should exit the resonance near an obliquity of  $180^\circ$ .

Which spin resonance is encountered by Styx first as Charon drifts away from Pluto? The two resonances are not on top of each other as the  $\sin^2 \theta$  resonance has argument with frequency  $\nu_{2j}\alpha_s = n_{Styx} - 3n_{Charon}$ , whereas for the  $\sin \theta \cos \theta$  resonance the argument frequency is  $\nu_{2jo}\alpha_s = n_{Styx} - 3n_{Charon} - \Omega_{Charon}$ . As  $\dot{\Omega}_{Charon} < 0$ , for an outward drifting Charon, Styx should encounter the  $\sin \theta \cos \theta$  resonance first and that may explain why the obliquity was lifted to near  $90^\circ$  in our simulations rather than  $180^\circ$  (see section 5 by [Quillen et al.(2017)]). At high obliquity, the  $\sin^2 \theta$  resonance could still be important. Perhaps this resonance, or evolution involving both perturbation terms could account for the higher than  $90^\circ$  obliquities of Nix and Hydra measured by [Weaver et al.(2016)].

With resonance strength  $\epsilon \sim 0.05$  the drift rate in the  $\sin \theta \cos \theta$  resonance (using equation 54)  $|\dot{\nu}_{2jo}| \lesssim 0.04$  and giving a constraint on the migration rate  $|\dot{n}| \lesssim 0.04\alpha_s^2$  or migration on a timescale  $t_{mig} \gtrsim 30 \left(\frac{n}{\alpha_s}\right)^2 n^{-1}$ . Here either

Charon can move away from Pluto or equivalently Styx could migrate inward. As discussed in section 2.4 of [Quillen et al.(2017)], the precession rate for all the minor satellites is  $\alpha_s \sim \frac{n}{2} \frac{P_s}{P_o}$  where  $\frac{P_s}{P_o}$  is the ratio of spin period to orbital period. Currently  $\frac{P_s}{P_o} \sim 6.2, 13.6$  for Styx and Nix, respectively. This gives a constraint on the migration timescale

$$t_{mig} = \frac{a}{\dot{a}} \gtrsim 30 \left( \frac{P_s}{P_o} \right)^2 P_o \quad (56)$$

or a few hundred times greater than the orbital period. This limiting migration rate is not slow and would be satisfied during an epoch of circumbinary disk evolution (e.g., [Kenyon & Bromley(2014)]). The total time required for the lift in obliquity to take place (using equation 55) would be only of order a hundred orbital periods or a few thousand years, easily satisfied, and consistent with the rapid obliquity lifts seen in our simulation. The extent of migration required is roughly the semi-major axis times the ratio  $P_s/P_o$  so is of order 1/6 the semi-major axis, taking Styx's current value for this ratio. If Charon migrates rather than Styx, the extent of migration required is lower due to the index 3 on  $\lambda_{Charon}$  in the resonant angle and on  $n_{Charon}$  in the associated frequency  $\nu_{2j}$ .

Nix is near the third order 4:1 mean motion resonance and the Hamiltonian we consider is that in equation 35. The terms that are important are the coefficients that are first order in eccentricity,  $c_{e_3}^1$  and  $c_{e'_3}^1$  and with  $j = 1$ . However this resonance is  $\propto \sin^2 \theta$  and our simulation showed resonance escape near an obliquity of  $\sim 90^\circ$ . We would attribute this behavior to higher order terms, such as proportional to  $es'$ , that we neglected from our computations in section 2.5. We have checked that the expansion to first order in  $es'$  (or  $e's'$ ) would give terms proportional to  $\sin \theta \cos \theta$  and with argument similar to a third-order mean motion resonance. For the 4:1 resonance, dependence on inclination and eccentricity for the  $\sin \theta \cos \theta$  term implies that the spin resonance strength would be weaker for Nix than Styx and so a slower migration rate and longer time would be needed to tilt Nix than Styx. However, the constraints on these quantities for Styx were easy to satisfy, so the mechanism for tilting Nix is also likely to be effective. If these spin resonances operated on Styx and Nix, the near  $90^\circ$  obliquities imply that Charon's orbit was relatively inclined during the migration as the strongest perturbation terms  $\propto \sin \theta \cos \theta$  are first order in orbital inclination.

Our toy model considers each resonant term separately, but likely both  $\sin^2 \theta$  and  $\sin \theta \cos \theta$  terms are present and simultaneously important for these spin resonances. We have not yet explored higher inclinations or slower migration rates in our mass-spring model simulations, leaving this for future work. At moderate inclination both Styx and Nix might initially be captured into a  $\sin \theta \cos \theta$  resonance but escape or could be subsequently pushed higher by a  $\sin^2 \theta$  resonance, possibly accounting for Nix's  $123^\circ$  [Weaver et al.(2016)] and higher than  $90^\circ$  obliquity.

Kerberos is near a 5:1 mean motion resonance with Charon and Hydra near a 6:1 mean motion resonance. Similar spin resonances could have operated on

both of these satellites. Our Hamiltonian models in sections 2.4 and 2.5 imply that the spin resonances near the 5:1 and 6:1 mean motion resonances would be higher than first order in inclination and eccentricity. They would be weaker, require slower migration rates for capture and longer time to evolve within resonance to lift the obliquities. Our previous numerical simulations did not show Kerberos tilted by the same spin resonance mechanism as Styx and Nix, but perhaps this is because we had not run longer simulations at slower migration rates (required for resonance capture because the spin resonances would be weaker). Since we only ran simulations of three bodies (Pluto, Charon and a satellite) satellite interactions were not present, however these can increase eccentricities or inclinations and the associated spin resonance strengths.

We previously speculated that a mean motion resonance between Nix and Hydra could affect Hydra's obliquity [Quillen et al.(2017)]. However the strength of such a resonance depends on the mass ratio of Nix and Pluto and this would make the spin resonances 4 to 5 orders of magnitude weaker than those involving Charon and so very weak. The resonance strengths computed here arise from the direct torque applied from a orbiting point mass, in this setting from Nix directly onto Hydra. Indirectly Nix could excite the orbit of Hydra due to a 3:2 first order mean motion resonance between them and the torque from Pluto and Charon arising from the orbit perturbations of Hydra might affect Hydra's spin. This perturbation would probably be weak as it also depends on the mass ratio of Nix and Pluto, however if important it would be most effective near a first order mean motion resonance such as the 3:2 mean motion resonance (first order in eccentricity and between Nix and Hydra), as discussed at the end of section 2.5). More likely is that interactions between the satellites increased the orbital eccentricities and inclinations making the spin resonance induced by Charon stronger.

## 5 Application to Uranus

The successful *Nice* model [Tsiganis et al.(2005)] and its variants (e.g., [Morbidelli et al.(2009), Nesvornyy(2011), Nesvornyy & Morbidelli(2012), Nesvornyy(2015), Deienno et al.(2017)]), postulate an epoch or epochs of planetary migration beginning with planets near or in mean motion resonance [Morbidelli et al.(2007)]. During planet migration, secular resonances and encounters between planets can alter planet spin orientation or obliquity [Ward & Hamilton(2004)]. Likewise the current obliquities of the giant planets could give clues about the extent and speed of planetary migration during early epochs of Solar system evolution (e.g., [Boué & Laskar(2010), Brasser & Lee(2015)]).

The large obliquity of Uranus has primarily been attributed to a tangential or grazing collision with an Earth-sized proto-planet at the end of the epoch of accretion (e.g., [Safronov(1969), Korycansky et al.(1990), Slattery et al.(1992), Lee et al.(2007), Parisi et al.(2008), Parisi(2011)]). However, [Boué & Laskar(2010)] proposed a collisionless scenario involving an additional, but now absent, satellite. Proposed is that a close encounter at the end of the era of migration ejected

this satellite while Uranus was at high orbital inclination, and following orbital inclination damping the planet was left at high obliquity. Drift of secular spin resonances, explaining Saturn’s obliquity, might also account for Uranus’s obliquity [Rogoszinski & Hamilton(2016)].

We consider the possibility that during an early epoch of planetary migration Uranus was captured into a mean motion resonance with another giant planet and while in it, its obliquity was lifted due to spin resonance. This scenario would give an alternative non-collisional scenario accounting for Uranus’s high obliquity. The spin resonance strengths (see equation 26) depend on the mass ratio of perturbing planet to that of the central star and this is at most the ratio of Jupiter’s mass to that of the Sun or  $\sim 10^{-3}$ . For Uranus external to its perturber, our parameter  $\beta$  is equal to this mass ratio. Using coefficients in Table 2 we estimate a 5:3 resonance strength  $\epsilon = \beta e_0^{j=3} \sim 2 \times 10^{-3}$ , a 4:3 resonance strength  $\epsilon = \beta e_1^{j=3} e_p \sim 6 \times 10^{-3} e_p$  with  $e_p$  the eccentricity of the inner perturbing planet. At most these coefficients are of order  $10^{-2}$  and so the spin resonance strengths are likely to be about 10 times weaker than we considered in the Pluto-Charon system. Equations 53 or 54 and 55 imply that the time required to lift Uranus would be of order 1000 times its precession period.

Taking into account its satellite system, Uranus’s precession period is currently approximately  $10^8$  years [Ward(1975)]. The precession period is so slow that there is not enough time during a *Nice* model epoch of planetary migration for the spin resonances considered here to tilt the planet. If Uranus had a much heavier and more extended satellite system [Mosqueira & Estrada(2003a), Mosqueira & Estrada(2003b)] then its precession period would be reduced. In this case we could consider capture into a 3:2, 4:3 or 5:3 resonance with Saturn and a spin resonance associated with one of these mean motion resonances. However the resonance strengths depend on eccentricity and inclination, making them even weaker. The time required to lift the planet remains long, of order the age of the Solar system, and requiring a timescale longer than the postulated era of migration. Uranus and Saturn migrating in such proximity are unlikely to remain stable but the spin resonance would require hundreds of spin precession periods to tilt Uranus. We conclude that the type of spin resonance explored here cannot account for Uranus’s high obliquity.

The spin secular resonance mechanism explored by [Ward & Hamilton(2004)] involves drift of secular spin resonance. The secular spin resonances are about the same size as the mean-motion/spin precession resonances. But Uranus currently is near a secular resonance, that associated with the vertical secular eigenfrequency associated with Neptune. The spin-secular resonance could have operated on a timescale of billions of years. For a mean-motion/spin precession resonance to operate the planet would need to be near a mean motion resonance for billions of years but Uranus is no longer near one and was probably not near or in one for as long a time period.

## 6 Summary and Discussion

We have explored a Hamiltonian model for the dynamics of the principal axis of rotation of an orbiting planet or satellite assuming that the spinning body remains rapidly spinning about its principal inertial axis. We have computed the torque exerted on the spinning body from a point mass also in orbit about the central mass (a star if the our spinning object is a planet or a planet if our spinning object is a satellite). Unlike many previous studies (e.g., [Colombo(1966)]), we do not average over the orbital period. We have computed perturbations from the orbiting point mass to first order in orbital inclinations and eccentricities (but not their product). The perturbation terms are either proportional to  $\sin^2 \theta$  or to  $\sin \theta \cos \theta$  with obliquity  $\theta$ . Taking a single Fourier component (of the perturbation) we derive the Hamiltonians for the spin orientation shown in equations 30, 35, and 36 that are relevant near second order, third order and first order mean motion resonances, respectively, but affect obliquity and spin precession rate. The resonant arguments for the resonance near a second order mean motion resonance in equation 30 are consistent with slowly moving angles (equation 1) we previously saw in numerical simulations of Styx when its obliquity varied [Quillen et al.(2017)]. Our Hamiltonian model provides a framework for estimating the strengths of spin resonances involving a mean motion resonance and the precession angle of a spinning body.

Numerical integrations of one of these one-dimensional Hamiltonians (equations 30, 35, or 36) containing a single resonant perturbation term show that if the resonance drifts, a spinning body initially at low obliquity can be captured into spin resonance and its obliquity lifted to near  $180^\circ$  or  $90^\circ$  depending upon whether the perturbation term is  $\propto \sin^2 \theta$  or  $\sin \theta \cos \theta$ . The  $\sin \theta \cos \theta$  requires non-zero orbital inclination of the spinning body with respect to the perturbing one. We estimate the maximum drift rate allowing spin resonance capture and the timescale required to reach the maximum obliquity when the body escapes resonance. Resonance capture into these spin resonances only takes place if the perturbing mass and spinning body have approaching orbits, similar to capture into mean motion orbital resonance.

We applied our Hamiltonian model to a migrating Pluto-Charon satellite system. The spin resonance seems capable of accounting for the large obliquity variations we previously saw in our simulations of the spin evolution of satellites Styx and Nix near the 3:1 and 4:1 mean motion resonances with Charon. Outward migration of Charon or inward migration of Styx and Nix could have let initially low obliquity Styx and Nix be captured into a spin resonance that lifted their obliquities. As Styx and Nix have obliquities near  $90^\circ$  and not near  $180^\circ$ , the capture would have involved a resonance proportional to  $\sin \theta \cos \theta$  and so requires Charon's orbit to be inclined by a few degrees with respect to the orbits of Styx and Nix. Due to Charon's large mass, the resonances are sufficiently strong that the constraints on the migration rate for resonance capture are loose and the time needed to tilt the satellites is short, of order only a thousand years. Similar spin resonances could operate on Kerberos and

Hydra, though they would be higher order in eccentricity and inclination and so weaker.

We explored whether Uranus could be tilted by a similar mechanism during an early epoch when Uranus might have been in a first order mean motion resonance with another giant planet such as Saturn. However Uranus’s spin precession period is long enough that tilting the planet would require billions of years. Since Uranus probably did not spend much time in or near mean motion resonance with another planet, this type of spin resonance is unlikely to account for Uranus’s current high obliquity.

As the giant planets in the Solar system are not currently in or near strong mean motion resonances, the mean-motion/spin precession resonance was justifiably neglected from previous studies. However the spin-resonances discussed here may be important in migrating rapidly spinning satellite and planetary systems, such as Pluto and Charon’s and possibly migrating compact exoplanet or satellite systems prior to tidal spin down. The approximate Hamiltonian model presented here could aid in interpretation of future simulations of spin evolution in such settings.

We explored toy Hamiltonian models containing a single resonant argument. However real systems are likely to be affected by multiple terms, each dependent on an argument that varies at a similar frequency. Spin evolution could be chaotic due to these nearby resonances. Interaction between the terms might allow resonance escape at obliquities between 90 and 180° possibly accounting for the 123° obliquity of Nix [Weaver et al.(2016)]. The spin resonances are important near mean motion resonances, and so future study of spin evolution where these spin resonances are important should also consider the orbital dynamics in or near mean motion resonance (e.g., [Voyatzis et al.(2014)]).

**Acknowledgements** We warmly thank our referee, Gwenaél Boué, for kindly finding and helping us correct our errors. Her time is very much appreciated. We gratefully acknowledge support from the Simons Foundation and the hospitality of the Leibniz Institut für Astrophysik, Postdam. BN acknowledges the financial support of the contract Prodex CR90253 from the Belgian Science Policy Office.

## References

- Bills(1990). Bills, B. G.: The Rigid Body Obliquity History of Mars. *J. Geophys. Res.* 96, B9, 14137–14153 (1990)
- Borderies & Goldreich(1984). Borderies, N., & Goldreich, P.: A simple derivation of capture probabilities for the  $j+1:j$  and  $j+2:j$  orbit-orbit resonance problems. *Celestial Mech.* 32, 127–132 (1984)
- Boué & Laskar(2006). Boué, G., & Laskar, J.: Precession of a planet with a satellite. *Icarus*, 185, 312–330 (2006)
- Boué & Laskar(2010). Boué, G., & Laskar, J.: A Collisionless Scenario for Uranus Tilting. *Astrophys. J. Letters* 712, L44–47 (2010)
- Brasser & Lee(2015). Brasser, R., and Lee, M. H.: Tilting Saturn without Tilting Jupiter: Constraints on Giant Planet Migration. *Astron. J.* 150, 157–175 (2015)
- Colombo(1966). Colombo G.: Cassini’s second and third laws. *Astron. J.* 71, 891–996 (1966)

- Correia et al.(2015). Correia, A. C. M., Leleu, A., Rambaux, N., & Robutel, P.: Spin-orbit coupling and chaotic rotation for circumbinary bodies; Application to the small satellites of the Pluto-Charon system. *Astron. & Astrophys.* 580, L14–21 (2015)
- Deienno et al.(2017). Deienno, R., Morbidelli, A., Gomes, R. S., & Nesvorny, D.: Constraining the Giant Planets? Initial Configuration from Their Evolution: Implications for the Timing of the Planetary Instability. *Astron. J.* 153, 153–166 (2017)
- Estrada & Mosqueira(2006). Estrada, P. R., & Mosqueira, I.: A gas-poor planetesimal capture model for the formation of giant planet satellite systems. *Icarus* 181, 486–509 (2006)
- French et al.(1993). French, R. G., Nicholson, P. D., Cooke, M. L., Elliot, J. L., Matthews, K., Perkovic, O., Tollestrup, E., Harvey, P., Chanover, N. J., Clark, M. A., Dunham, E. W., Forrest, W., Harrington, J., Pipher, J., Brahic, A., Grenier, I., Roques, F., and Arndt, M.: Geometry of the Saturn system from the 3 July 1989 occultation of 28 SGR and Voyager observations. *Icarus* 103, 163–214 (1993)
- Frouard et al.(2016). Frouard, J., Quillen, A. C., Efroimsky, M., & Giannella, D.: Numerical Simulation of Tidal Evolution of a Viscoelastic Body Modelled with a Mass-Spring Network. *Mon. Notices of the Royal Astron. Society* 458, 2890–2901 (2016)
- Goldreich(1965). Goldreich, P.: Inclination of satellite orbits about an oblate precessing planet. *Astron. J.* 70, 5–9 (1965)
- Goldreich & Toomre(1969). Goldreich, P. and Toomre, A.: Some Remarks on Polar Wandering. *J. Geophys. Res.* 74, 2555–2567 (1969)
- Goldreich & Peale(1966). Goldreich, P., & S. J. Peale, S. J.: Spin-orbit coupling in the solar system. *Astron. J.* 71, 425–438 (1966)
- Hamilton & Ward(2004). Hamilton, D. P., & Ward, W. R.: Tilting Saturn. II. Numerical Model. *Astron. J.* 128, 2510–2517 (2004)
- Kenyon & Bromley(2014). Kenyon, S. J., & Bromley, B. C.: The Formation of Pluto’s Low-Mass Satellites. *Astron. J.* 147, 8–25 (2014)
- Korycansky et al.(1990). Korycansky, D. G., Bodenheimer, P., Cassen, P., & Pollak, J. B.: One-dimensional calculations of a large impact on Uranus. *Icarus* 84, 528–541 (1990)
- Laskar & Robutel(1993). Laskar, J., & Robutel, P.: The chaotic obliquity of the planets. *Nature* 361, 608–612 (1993)
- Lee et al.(2007). Lee, M. H., Peale, S. J., Pfahl, E., & Ward, W. R.: Evolution of the obliquities of the giant planets in encounters during migration. *Icarus* 190, 103–109 (2007)
- Morbidelli et al.(2007). Morbidelli, A., Tsiganis, K., Crida, A., Levison, H. F., & Gomes, R.: Dynamics of the Giant Planets of the Solar System in the Gaseous Protoplanetary Disk and Their Relationship to the Current Orbital Architecture. *Astron. J.* 134, 1790–1798 (2007)
- Morbidelli et al.(2009). Morbidelli, A., Brasser, R., Tsiganis, K., Gomes, R., & Levison, H. F.: Constructing the secular architecture of the solar system I. The giant planets. *Astron. & Astrophys.* 507, 1041–1052 (2009)
- Mosqueira & Estrada(2003a). Mosqueira, I., & Estrada, P. R.: Formation of the regular satellites of giant planets in an extended gaseous nebula I: subnebula model and accretion of satellites. *Icarus* 163, 198–231 (2003)
- Mosqueira & Estrada(2003b). Mosqueira, I., & Estrada, P. R.: Formation of the regular satellites of giant planets in an extended gaseous nebula II: satellite migration and survival. *Icarus* 163, 232–255 (2003)
- Murray & Dermott(1999). Murray, C.D. & Dermott, S.F.: *Solar System Dynamics*, Cambridge University Press, Cambridge (1999)
- Mustill & Wyatt(2011). Mustill, A. J., and Wyatt, M. C.: A general model of resonance capture in planetary systems: first- and second-order resonances. *Mon. Notices of the Royal Astron. Society* 413, 554–572 (2011)
- Nesvorny(2015). Nesvorny, D.: Evidence for Slow Migration of Neptune from the Inclination Distribution of Kuiper Belt Objects. *Astron. J.* 150, 73–91 (2015).
- Nesvorny(2011). Nesvorny, D.: Young Solar System’s Fifth Giant Planet? *Astrophys. J.* 742, L22–27 (2011)
- Nesvorny & Morbidelli(2012). Nesvorny, D., and Morbidelli, A.: Statistical Study of the Early Solar System’s Instability with Four, Five, and Six Giant Planets. *Astron. J.* 144, 117–136 (2012)
- Noyelles et al.(2014). Noyelles, B., Frouard, J., Makarov, V.V., and Efroimsky, M.: Spin-orbit evolution of Mercury revisited. *Icarus* 241, 26–44 (2014)

- Parisi et al.(2008). Parisi, M. G., Carraro, G., Maris, M., & Brunini, A.: Constraints to Uranus' great collision IV. The origin of Prospero. *Astron. & Astrophys.* 482, 657–664 (2008)
- Parisi & del Valle(2011). Parisi, M. G., & del Valle, L.: Last giant impact on the Neptunian system. Constraints on oligarchic masses in the trans-Saturnian region. *Astron. & Astrophys.* 530, A46 (2011)
- Parisi(2011). Parisi, M. G.: Last giant impact on Uranus. Constraints on oligarchic masses in the trans-Saturnian region. *Astron. & Astrophys.* 534, A28 (2011)
- Quillen et al.(2017). Quillen, A. C., Nichols-Fleming, F., Chen, Y.-Y. and Noyelles, B.: Obliquity evolution of the minor satellites of Pluto and Charon. *Icarus* 293, 94–113 (2017)
- Quillen(2006). Quillen, A. C.: Reducing the probability of capture into resonance. *Mon. Notices of the Royal Astron. Society* 365, 1367–1382 (2006)
- Rogoszinski & Hamilton(2016). Rogoszinski, Z., & Hamilton, D. P.: Tilting Uranus without a Collision. *American Astronomical Society, DPS meeting #48*, id. 318.09 (2016)
- Safronov(1969). Safronov, V. S.: Evolution of the Protoplanetary Cloud and Formation of the Earth and the Planets. NASA TTF-677 (1969)
- Slattery et al.(1992). Slattery, W. L., Benz, W., & Cameron, A. G. W.: Giant impacts on a primitive Uranus. *Icarus* 99, 167–174 (1992)
- Tsiganis et al.(2005). Tsiganis, K., Gomes, R., Morbidelli, A. & Levison, H. F.: Origin of the orbital architecture of the giant planets of the Solar System. *Nature* 435, 459–461 (2005)
- Touma & Wisdom(1993). Touma, J., & Wisdom, J.: The chaotic obliquity of Mars. *Science* 259, 1294–1297 (1993)
- Voyatzis et al.(2014). Voyatzis, G., Antoniadou, K. I., and Tsiganis, K.: Vertical instability and inclination excitation during planetary migration. *Celestial Mechanics Dynamical Astron.* 119, 221–235 (2014)
- Ward(1973). Ward, W. R.: Large-scale variations in the obliquity of Mars. *Science* 181, 260–262 (1973)
- Ward(1974). Ward, W.R.: Climatic variations on Mars: I. Astronomical theory of insolation. *J. Geophys. Res.* 79, 3375–3386 (1973)
- Ward(1975). Ward, W.R.: Tidal friction and generalized Cassini's laws in the solar system. *Astron. J.* 80, 64–70 (1975)
- Ward & Hamilton(2004). Ward, W. R., & Hamilton, D. P.: Tilting Saturn. II. Analytical Model. *Astron. J.* 128, 2501–2509 (2004)
- Ward(1979). Ward, W. R.: Present obliquity oscillations of Mars: Fourth-order accuracy in orbital  $e$  and  $I$ . *J. Geophys. Res.* 114, 237–241 (1979)
- Ward & Rudy(1991). Ward, W. R., and Rudy, D. J.: Resonant obliquity of Mars? *Icarus* 94, 160–164 (1991)
- Ward & Canup(2006). Ward, W. R., & Canup, R. M.: The Obliquity of Jupiter. *Astrophys. J. Letters* 640, L91–L94 (2006)
- Weaver et al.(2016). Weaver, H. A., Buie, M. W., Buratti, B. J., Grundy, W. M., Lauer, T. R., Olkin, C. B., Parker, A. H., Porter, S. B., Showalter, M. R., Spencer, J. R., Stern, S. A., Verbiscer, A. J., McKinnon, W. B., Moore, J. M., Robbins, S. J., Schenk, P., Singer, K. N., Barnouin, O. S., Cheng, A. F., Ernst, C. M., Lisse, C. M., Jennings, D. E., Lunsford, A. W., Reuter, D. C., Hamilton, D. P., Kaufmann, D. E., Ennico, K., Young, L. A., Beyer, R. A., Binzel, R. P., Bray, V. J., Chaikin, A. L., Cook, J. C., Cruikshank, D. P., Dalle Ore, C. M., Earle, A. M., Gladstone, G. R., Howett, C. J. A., Linscott, I. R., Nimmo, F., Parker, J. Wm., Philippe, S., Protopapa, S., Reitsema, H. J., Schmitt, B., Stryk, T., Summers, M. E., Tsang, C. C. C., Throop, H. H. B., White, O. L., Zangari, A. M.: The Small Satellites of Pluto as Observed by New Horizons. *Science* 351, 1281, (2016) DOI: 10.1126/science.aae0030
- Wisdom et al.(1984). Wisdom, J., Peale, S. J., & Mignard, F.: The Chaotic Rotation of Hyperion. *Icarus* 58, 137–152 (1984)